Ultrahigh Fluence Radiation Monitoring Technology for the Future Circular Collider at CERN

Georgi Gorine, *Student Member, IEEE*, Giuseppe Pezzullo, Igor Mandic, Anže Jazbec, Luka Snoj, Mar Capeans, Michael Moll, Didier Bouvet, Federico Ravotti, *Member, IEEE*, and Jean-Michel Sallese, *Member, IEEE*

***Abstract*— The future circular collider (FCC) is foreseen as the next-generation ∼100-km long synchrotron to be built in the Geneva area starting 2050. This machine is expected to reach an energy level of 100 TeV generating unprecedented radiation levels >100 times higher than in today's large hadron collider (LHC). Current radiation monitoring system, like the RADMONs employed in the LHC, will not be capable to function and withstand this harsh environment. The development of a new ultrahigh fluence and dose radiation sensor is a key element to allow irradiation tests of FCC equipment and, at a later stage, to monitor radiation levels in the FCC itself. In this paper, we present an innovative dosimetry solution based on thin layers of metals, which resistivity is shown to increase significantly due to the accumulated displacement damage. After describing the fabrication techniques used to manufacture these radiation-dependent resistors, we show and discuss the results of the irradiation experiments carried out with neutrons (up to 10^{18} n/cm^2 at the JSI TRIGA reactor) and with protons (up to 5.2×10^{16} p/cm^2 at CERN IRRAD Facility) to validate the proposed concept of possible ultrahigh fluence FCC dosimeter.**

***Index Terms*— Displacement damage, dosimetry, electrical characterization, future circular collider (FCC), neutron radiation effects, nonionizing energy loss (NIEL), proton radiation effects, radiation effects, radiation facilities, radiation monitoring.**

I. Introduction

THE future circular collider (FCC) is being designed to reach h-h collisions at an unprecedented collision energy levels of 100 TeV, about 8 times higher than in today's large hadron collider (LHC). Because of the increased energy and luminosity, during ten years of FCC operation, radiation levels will likely reach tens of kGy (with $>10^{15}$ particles/cm^2) in certain sections of the FCC tunnel [1], and exceed several tens of MGy (with $>10^{17}$ particles/cm^2) inside the FCC experiments [2]. These estimations correspond to factors of 1000 (and 100) with respect to the expected conditions at LHC and high-luminosity LHC (HL-LHC), respectively [3]. To withstand such a harsh radiation environment, special materials and technologies are required. This implies strict components selection and development of custom qualification protocols taking into account possible dependencies of the radiation response to different technologies [4].

A survey of state-of-the-art solid-state devices for radiation measurement showed that the current existing technologies are not capable of integrating such radiation levels, as well as of providing feasible solutions to build an online radiation monitor fulfilling the FCC requirements. For these reasons, a completely novel dosimetry technology is under development as potential solution for ultrahigh particle fluence monitoring. The proposed innovative solution consists of thin-film metal structures, for which the resistivity varies according to the integrated particle fluence. The sensitivity to displacement damage can then be trimmed by varying geometrical (thickness, width W, and length L) and physical (material) properties of the thin layers. The microfabrication of the devices was carried out at the Centre of Micronanotechnology (CMi), Ecole Polytechnique Fédérale de Lausanne (EPFL), Lausanne, Switzerland, and specific high-fluence irradiation tests, with high-energy neutrons and protons, have been performed in facilities at CERN, Geneva [5], and the Jožef Stefan Institute (JSI), Ljubljana, Slovenia [6].

This paper is structured as follows. Section II gives an overview of the existing solid-state dosimeters as well as a description of the proposed dosimetry technology. Section III covers the Monte Carlo simulations covering the calculations of radiation damage on metals. Section IV describes the device fabrication and printed-circuit board (PCB) production, as well as different irradiation tests. Section V focuses on results of the irradiation tests. Section VI covers the discussion and Section VII gives conclusions and outlines future work.

II. Dosimetry Technology

Current solid-state dosimeters employed at the high-energy physics experiments at the CERN LHC and in the accelerator tunnel itself are based on the so-called RADMON devices (PH-RADMON, developed within the CERN Physics (PH) Department targeting the needs of LHC experiments [7] and LHC-RADMON for the tunnel areas [8]). These radiation

Manuscript received September 29, 2017; revised December 1, 2017; accepted January 14, 2018. Date of publication January 24, 2018; date of current version August 15, 2018. This work was supported in part by CERN Future Circular Collider, Special Technologies, Radiation Hardness Assurance, Work Package 11, and in part by the European Union's Horizon 2020 Research and Innovation Programme through the H2020 Project AIDA-2020 Transnational Access under Grant 654168.

G. Gorine is with CERN EP-DD-DT, 1211 Geneva, Switzerland, and also with the École Polytechnique Fédérale de Lausanne, GR-SCI-IEL, 1015 Lausanne, Switzerland (e-mail: Georgi.Gorine@cern.ch).

G. Pezzullo, M. Moll, and F. Ravotti are with CERN EP-DD-DT, 1211 Geneva, Switzerland.

M. Capeans is with CERN TE-PPR, 1211 Geneva, Switzerland.

I. Mandic is with the Experimental Particle Physics Department, Jožef Stefan Institute, 1000 Ljubljana, Slovenia.

A. Jazbec and L. Snoj are with the Reactor Physics Department, Jožef Stefan Institute, 1000 Ljubljana, Slovenia.

D. Bouvet is with CMI-GE, École Polytechnique Fédérale de Lausanne, 1015 Lausanne, Switzerland.

J.-M. Sallese is with GR-SCI-IEL, École Polytechnique Fédérale de Lausanne, 1015 Lausanne, Switzerland.

Color versions of one or more of the figures in this paper are available online at http://ieeexplore.ieee.org.

Digital Object Identifier 10.1109/TNS.2018.2797540

TABLE I

OPERATIONAL RANGE OF CURRENT PH-RADMON DEVICES FOR THE LHC EXPERIMENTS [7]

Device	Type	Energy Loss	Operating Range
LAAS	RadFET	Ionizing [Gy]	0.01 – 10
REM	RadFET	Ionizing [Gy]	10 – 100k
LBSD	p-i-n diode	Non Ionizing [n_{1MeV}/cm^2]	$1x10^8$ - $2x10^{12}$
BPW	p-i-n diode	Non Ionizing [n_{1MeV}/cm^2]	$2x10^{12}$ - $1x10^{15}$

TABLE II

MAX FLUENCE AND DOSE LEVELS AT CERN ACCELERATORS (AFTER TEN YEARS OF OPERATION) [1], [2]

Experiment	Luminosity [ab^{-1}]	Fluence[n_{1MeV}/cm^2]	Dose [MGy]
LHC	0.3	1.0×10^{15}	0.1
HL-LHC	3	1.5×10^{16}	4.8
FCC	3	2.8×10^{16}	9
FCC	30	2.8×10^{17}	90

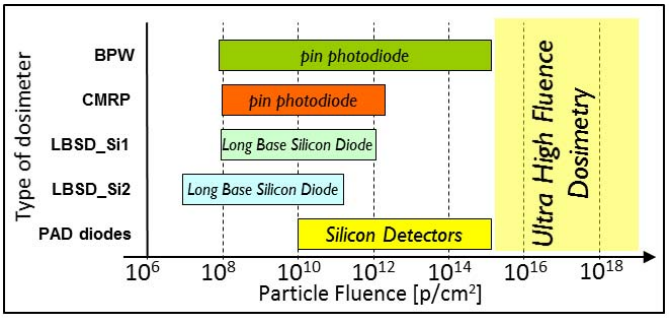

Fig. 1. Different solid-state NIEL dosimetries available on the market are shown with respect to their monitoring range. The highlighted and empty area in the ultrahigh fluence range indicates the target area of the technology presented in this paper.

monitoring systems are assembled with several specialized sensors, each capable of monitoring different types of radiation with different sensitivities and dynamic ranges [9]. As listed in Table I, RadFETs are used for measuring ionizing radiation by means of the increase of their threshold voltage due to charge trapping in the thick gate oxide. Selected p-i-n diodes are instead used for measuring fluence levels by correlating them with the increase of forward voltage due to displacement damage induced in the thick silicon base.

For both technologies, the key parameter is the thickness of the active layer, which directly affects the sensitivity and the operational range of the dosimeter (RadFETs with gate oxide thickness between 0.13 and 1.6 μm, and p-i-n diodes with base thickness between 210 to 1000 μm [9]).

For the FCC, the maximum expected integrated dose and fluence over ten years of operation are shown in Table II. These values can be compared with the range covered by the PH-RADMON sensor in Table I. The noticeable limitation of the technology currently employed in the LHC, and the clear absence of any other adequate radiation monitoring device for fluence monitoring (as depicted in Fig. 1), has pushed toward the research and development of a novel technology. At first, our focus has been on technologies for ultrahigh fluence monitoring to upgrade the current PH-RADMON and cover the whole FCC operational range from $>10^{15}$ particles/cm^2 up to 3×10^{17} particles/cm^2. The innovative approach has been to exploit thin layers of metal instead of silicon, like in current nonionizing energy loss (NIEL) dosimeters [10]. Such choice was driven by the fact that submicrometer thin layers of metals are known to be less sensitive to low particle fluences (where silicon layers would be), but at the same time, sensitive to very high fluence, where structural and electrically observable effects occur. Such property variations like changes in the material stiffness, generation of internal voids, surface swelling, and other, have been documented in [11]–[13]. In fact, displacement damage in metals is a known effect extensively studied in the past while developing materials and technologies for nuclear power plants [14] and space applications [15]. In the core of nuclear reactors, the particle flux can easily exceed 10^{15} n/cm^2/s, drastically increasing the probability of having atoms knocked from their initial positions in the crystal structures. This effect is usually expressed in units of displacement per atom (DPA). The DPA accounts for how often atoms in an irradiated material are displaced due to an impinging particle (see Section III).

Several studies were made to correlate the number of vacancies and interstitials produced by the nonionizing radiation with the change electrical resistivity of the material [16]–[18]. Similar resistivity measurements were also used for the characterization of metals irradiated in reactors. The resulting experimental data have shown that the resistivity increase as function of particle fluence can be expressed by two specific components: one log dependent, as result of the creation of defects in the lattice due to fast neutrons, and one linear as result of the transmutation mainly due to thermal neutrons [19].

Our proposed idea is therefore to profit of the resistivity variation in metals when exposed to high particle fluence, and to accomplish the FCC operational range and sensitivity requirements, by varying the dosimeter geometry (W, L, and thickness), using thin-film technologies.

The proposed sensor shown in Fig. 2, hereafter called radiation-dependent resistor (RDR), was made by sputtering thin layers of metal on silicon wafers and consecutive lithography and etching, into "serpentine-shaped" resistive structures covering an area of 3×3 mm^2, as schematized in Fig. 2(c). The selected materials for the produced RDRs were aluminum, chromium, and copper.

As shown in Table III, these three metals differ by their atomic number, as well as by their different crystallographic systems (body-centered cubic (bcc) chromium and face-centered cubic (fcc) copper and aluminum) [20]. Both characteristics have a strong impact on the defects production efficiency. The former because higher atomic number implies a greater amount of atoms thus increasing the interaction probability, the latter because fcc metals have a more compact lattice structure, consequently generating greater clusters, than the more open lattice of bcc metals [18]. More practically, the metals (aluminum, chromium, and copper), were chosen also for their suitable properties for microfabrication, such as

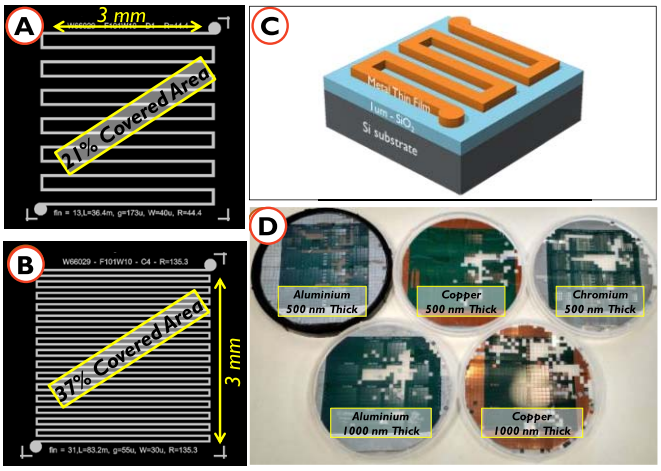

Fig. 2. Example of layout of (a) 3×3 mm^2 RDR with 13-finger 40 µm wide covering 21% of the whole chip area and (b) RDR with 31-finger 30 µm wide covering 37% of the area. A larger covered area may affect the overall device sensitivity. (c) Schematic cross section of one RDR showing the stack silicon substrate/SiO_2/metal. (d) Photograph of five produced wafers, with some of the chips removed for the electrical characterization.

TABLE III
MATERIAL COMPOSITION OF THE RDRS AND SIMULATED DPA*

Material	Atomic Number	Lattice Structure	DPA Neutrons [DPA/(n/cm^2)]	DPA Protons [DPA/(p/cm^2)]
Aluminum (Al)	13	fcc	3.21×10^{-20}	0.75×10^{-21}
Chromium (Cr)	24	bcc	1.91×10^{-20}	2.61×10^{-21}
Copper (Cu)	27	fcc	1.74×10^{-20}	3.85×10^{-21}

**Simulations performed with FLUKA considering a target of 1x1x0.1 mm^3 with neutron energy spectrum of the TRIGA nuclear reactor* [34]*, and 23 GeV protons.*

self-passivating, good adhesion with SiO_2-covered substrate, bondability (Al on Cr for wire-bonding pads), availability as targets for the sputtering machine, and also their relatively low level of induced radioactivity with respect to metals with even higher atomic number [21]. Table III also enlists the results obtained from radiation damage simulations, discussed in Section III.

III. SIMULATION DETAILS

Prior the realization of the first RDR prototypes, simulations were performed in order to assess the amount of displacement damage induced by extreme particle fluence in the different selected materials. Popular simulators used for calculating the radiation-matter interaction, such as SRIM [22], could not be used due to their intrinsic limitation to ions of energies below 2 GeV (high-energy protons in IRRAD are at 23 GeV, see Section IV-D), but also due to a nonconvergence in targets where the nuclear interaction length is much smaller than the target thickness. For these reasons, the FLUKA Monte Carlo tool [23], [24] has been used. The FLUKA scorecard used for the DPA calculation is DPA-SCO [25], and it accounts for every atom displaced from its initial location in the lattice, due to a primary or secondary impinging particle which recoil energy is higher than the lattice binding energy. For solving this calculation, FLUKA uses the theory of Norgett *et al.* [26],

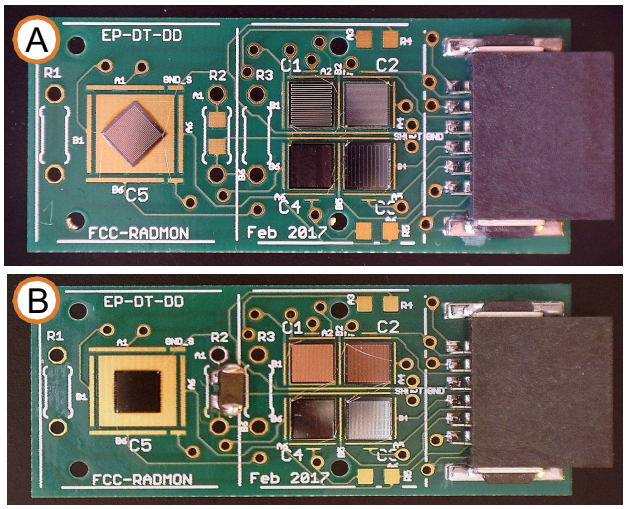

Fig. 3. Photograph of two FCC-RADMONs produced on a Doosan DS-7402 Hal-Free 0.2-mm substrate. (a) PCB for the neutron irradiation with five wire-bonded RDRs, one for each wafer shown in Fig. 2(c). (b) PCB for the proton irradiation, also with five RDRs and an extra onboard NTC temperature sensor mounted in position R2.

where both displacement efficiency and lattice displacement energy are taken into account. While the RDR sensors, as previously described, have a size of 3×3 mm^2 with a thickness of either 500 or 1000 nm, the target chosen for the simulation is of 1×1 mm^2 and 100 µm thickness, to reach faster convergence. In the end, the DPA has been normalized per incoming particle (n^0 and p^+) per cm^2. Table III lists these simulation results in terms of total DPA integrated over the entire irradiation spectrum (for neutrons, the one of the central irradiation channel of the JSI TRIGA nuclear reactor, and for protons the one of the IRRAD Proton Facility. See Sections IV-C and IV-D). From the simulated data, there was no straightforward conclusion on which material could offer better performance as dosimeter. For this reason, we decided to follow an empirical approach for this paper, by producing and characterizing metal nanostructures with irradiation experiments.

IV. EXPERIMENTAL DETAILS

A. Device Fabrication

The devices discussed in this paper have been fully fabricated in the cleanroom facilities of CMi, EPFL, Lausanne [27].

A total number of five 100-mm diameter wafers were produced varying the metal type (Al, Cr, and Cu), and the metal thickness (500 and 1000 nm), as shown in Fig. 2(c). Up to 300 devices were obtained on each wafer, but this number could be increased to 3000 by removing the test structures and covering the whole wafer area. The single die size was 3×3 mm^2 designed to be compatible with the hosting (PCB) shown in Fig. 3 and described in Section IV-B. The chosen "serpentine-shaped" layout of the chips shown in Fig. 2(a) and (b), allowed obtaining, in a limited area, resistance values ranging from few ohms to several kiloohms by increasing the number of fingers (2 to 51) and by varying their width W (from 2 to 50 µm) while keeping a fixed length L of 3 mm. At the end of the fabrication process,

TABLE IV
INITIAL RESISTANCE VALUES OF RDRS ON THE FOUR FCC-RADMON PCBS BEFORE IRRADIATION AT JSI AND IRRAD

Material:	Al	Cr	Cu	Al	Cu
PCB1-JSI	621.9 Ω	1502.5 Ω	148.2 Ω	525.7 Ω	141.7 Ω
PCB2-JSI	211.0 Ω	906.4 Ω	67.9 Ω	242.9 Ω	55.4 Ω
PCB1-IRRAD	29.1 Ω	838.3 Ω	50.4 Ω	51.0 Ω	29.6 Ω
PCB2-IRRAD	49.2 Ω	1502.2 Ω	56.2 Ω	116.9 Ω	29.7 Ω

the wafers have been diced and a set of dies has been measured using a probe station at CERN. The selected dies have been wire bonded (following a four-wire readout schema) on the FCC-RADMON PCB to allow online measuring of the resistance variation while testing at different irradiation facilities.

B. Sensor Carrier for Ultrahigh Fluence Experiments

For compatibility reasons, the newly made PCB-targeting FCC-fluence levels, shown in Fig. 3, follows the same layout of the integrated sensors carrier [28] currently employed for the PH-RADMON installed in the LHC experiments (from which the name FCC-RADMON was chosen), and it mainly differs by the chosen substrate material. This upgrade over standard FR4 PCBs was needed after experiencing surface corrosion during another irradiation test with a high proton fluence exceeding 2×10^{16} p/cm^2 in the IRRAD Proton Facility. The new selected material is a halogen-free and low-phosphorus content substrate produced by Doosan (DS-7402) [29]. The FCC-RADMON PCB offers space for bonding up to four 3×3 mm^2 and one 5×5 mm^2 chips, along with several positions for discrete through-hole and surface mount device components (such as an on-board negative temperature coefficient (NTC) sensor) In the PCB configurations shown in Fig. 3, five RDRs were mounted and wire bonded on each PCB following a four-wire measurement schema. (RDR initial values are listed in Table IV.) The connection is then performed with a 12 channel IDC cable using the same ERNI connector as the current PH-RADMON system [7]. Until now, the produced PCBs have been successfully irradiated up to 1×10^{18} neutrons/cm^2 in a TRIGA nuclear reactor and $>5 \times 10^{16}$ protons/cm^2 with a collimated 23-GeV proton beam, without showing any failures.

C. Neutron Irradiation at Jožef Stefan Institute

The produced RDRs were first tested in a neutron irradiation experiment at the TRIGA MARK II Nuclear Reactor of JSI, Ljubljana [30]. In about 40 hours, over five days of irradiation, a total neutron fluence of 1×10^{18}n/cm^2 has been reached in the central channel (CC) of the reactor, operated at a power of 250 kW. A photograph of the reactor pool is shown in Fig. 4(a). The broad neutron spectrum of the reactor is well characterized and stable during operation [6]. The following value has been used as reference flux for the CC at 250 kW: 7.2×10^{12} n/cm2/s calibrated using standard silicon diode dosimeters before starting our irradiation.

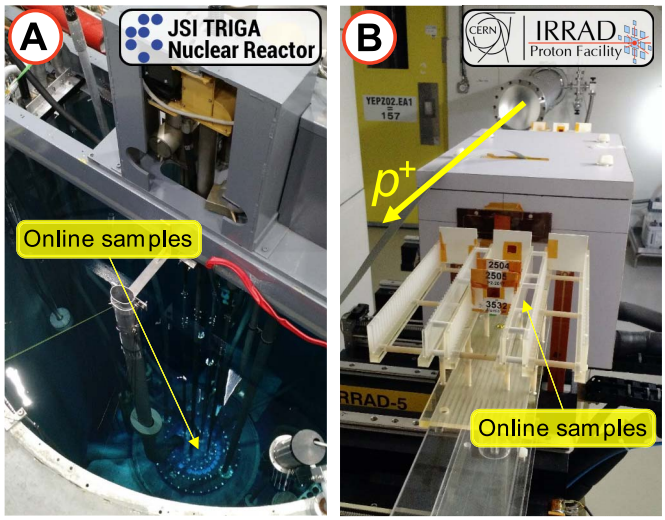

Fig. 4. (a) Top view of the 5-m deep JSI TRIGA reactor pool. The two FCC-RADMON boards were irradiated in the CC pointed by the arrow. (b) Photograph of the Zone 1 inside the CERN IRRAD Proton Facility. The two FCC-RADMON boards were mounted on cardboard holders and positioned on the IRRAD7 motorized table, here ready to be inserted into beam position.

Two FCC-RADMON boards, like the one in Fig. 3(a), taped with Kapton back to back, were inserted in a standard aluminum cylindrical sample holder to ensure mechanical protection during the insertion in the irradiation channel. Using two 12-channel IDC cables, the RDRs were connected to a test-bench located on the platform of the reactor, allowing an active readout of ten RDRs during the whole irradiation period (although a failure of the cable in the final stage of the irradiation limited the sampled data up to 9.4×10^{17}n/cm^2). These resistance measurements have been performed using a dedicated LabVIEW test-bench controlling an Agilent 34970A equipped with a 34901A switch matrix and a Keithley 2410 Source and Measure Unit (SMU). The switch matrix allowed to address each of the RDR under test and to connect them to the SMU for the four-wire measurement to take place.

D. Proton Irradiation at CERN-IRRAD

Starting from June 2017, two similar FCC-RADMONs mounting the same set of previously described RDRs and an extra NTC temperature probe [Fig. 3(b)] are being irradiated at the CERN Proton Irradiation Facility IRRAD [5]. As for the previously mentioned irradiation experiment, also in this case a dedicated LabVIEW test-bench was installed to allow an online monitoring of the RDRs resistance variation. After preparing the FCC-RADMONs on a cardboard holder, they were installed inside the IRRAD Proton Facility, as shown in Fig. 4(b).

The irradiation is performed with a Gaussian ($\sigma \sim 10$ mm) pulsed 23-GeV proton beam extracted from the Proton Synchrotron accelerator. Each spill, sent every 10 s, has a typical duration of 400 ms and contains on average $\sim 5 \times 10^{11}$ p/spill. Such flux allows reaching the HL-LHC required maximum fluence of 1.5×10^{16} n/cm^2 in less than two weeks, while

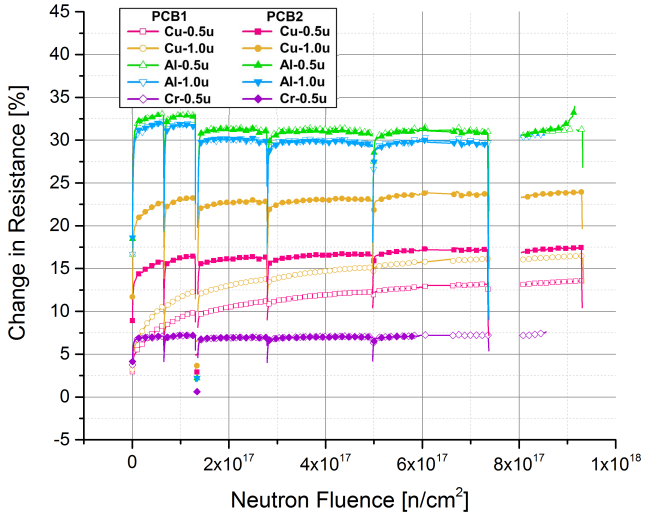

Fig. 5. Resistance variation from the initial value in percentage versus the integrated neutron fluence, for each RDR with 0.5- and 1-μm thickness, on PCB1 and PCB2. The negative peaks correspond to the overnight ON–OFF–ON transitions of the reactor induced by abrupt changes in temperature. The void before 8×10^{17} n/cm^2 is due to data loss during acquisition while the interrupted curves toward the end of the irradiation are probably due to a failure of the cable at 9.4×10^{17} n/cm^2.

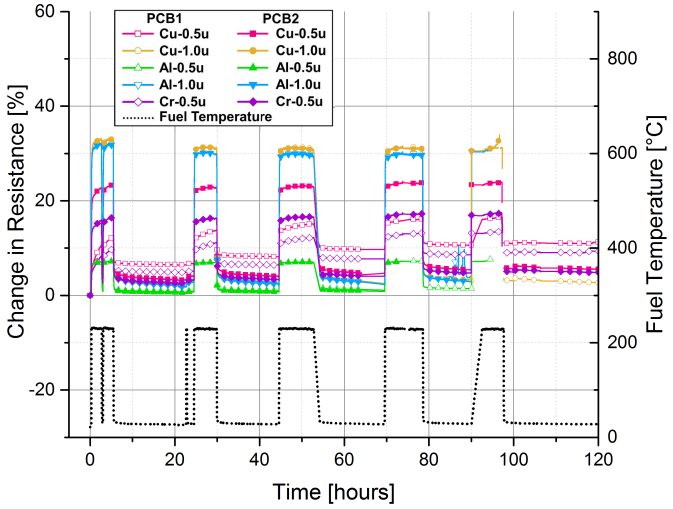

Fig. 6. Resistance variation from the initial value in percentage (left y-axis) compared with the temperature variations of the fuel elements of the reactor (black) over all the five days (120 h) of irradiation test (right y-axis). The points where the black curve is low at 25 °C correspond to the overnight stops where the reactor was switched OFF, while all the RDRs either experienced annealing (like the Al and Cr samples) or stayed flat (like the Cu samples).

it takes about an entire year (∼10 months) of continuous irradiation to reach the final FCC fluence of 2.8×10^{17} n/cm^2.

The dosimetry over such long irradiation experiment is performed by interposing pure aluminum foils in front of the FCC-RADMONs under irradiation [as shown in Fig. 4(b)] and replacing them every two weeks. Afterward, a gamma spectrometry of the irradiated foil allows estimating the proton fluence by counting the ^{22}Na activity in the foil as result of spallation reactions induced by the 23-GeV proton beam [31].

Even though the irradiation experiment will continue till the end of the 2017 CERN accelerators run, the preliminary data collected during three months, between June 7, 2017 and September 7, 2017, is shown and discussed in this paper. In such period a total proton fluence of 5.2×10^{16} p/cm^2 was reached.

V. Irradiation Test Results

A. Neutron Irradiation at Jožef Stefan Institute

The two FCC-RADMONs were inserted inside the CC before turning ON the reactor and measurements of every dosimeter were taken every minute. In Fig. 5, the change in resistance of all the measured RDRs is shown against the increasing total integrated neutron fluence. Only data points sampled when the reactor was ON are plotted.

All devices have shown a significant change with resistance values increased by 5% for the chromium samples, and up to 30% for the aluminum samples. However, such abrupt rise of resistance is not only induced by displacement damage, but mainly by the temperature variation in the irradiation channel. This correlation with temperature can clearly be seen in Fig. 6, where the temperature variation of the reactor fuel (dotted line) sampled over 120 hours, has been compared with the signal from the measured RDRs. The intermittent sudden decreases (and increases) in resistance value perfectly correspond to the points when the reactor was being driven from full power to zero (and back). Unfortunately, in this experiment, the FCC-RADMON boards did not include a temperature sensor due to the limited number of available channels on the PCB (12 total channels: ten used for V_{sense} and V_{force} of five RDRs and two channels for shared GND_{sense} and GND_{force}). For that reason, successive measurements were performed in the same channel using a PT100 sensor contained in a similar aluminum cylinder. This test, performed during 2 hours of operation at full power, has shown an inner channel temperature rising from about 25 °C to >65 °C rapidly after reaching reactor criticality. Also a temperature drift of about 0.5 °C/h (with reactor at full power) has been observed. Such temperature variations are clearly affecting the resistance value of all the RDRs, as visible in Fig. 5 (negative spikes), and in Fig. 6 (the square wave, corresponding to the overnight shutdowns of the reactor). While the damage was not permanent for the aluminum and chromium samples, where the overnight annealing lead to almost full recovery, the copper RDRs (Cu-0.5u and Cu-1.0u of PCB1) have shown a very promising result. As observable in Fig. 6, no loss in the monitored dosimetry quantity is occurring once the reactor restarts. This is further confirmed, by the overnight almost-flat plateau (longer segments between square waves), where no considerable annealing is occurring. In fact, the resistance value goes back to the value it was before the night stop, and continues then to grow with increasing fluence.

At the end of the irradiation week, the two copper RDR devices have shown an overall increase of resistance of 16.5% and 13.5% with respect to their initial values. Such increase was substantially higher during the first hours of irradiation (up to 1×10^{17} n/cm^2), where the sensitivity of the two copper RDRs of PCB1 was of ∼7.7 Ω/Φ_n

(1000-nm-thick RDR) and ~5.6 Ω/Φ_n (500-nm-thick RDR) with $\Phi_n = 10^{17}$ n/cm^2. However, close to the end of the irradiation (from 5×10^{17} to 1×10^{18} n/cm^2) the resolution dropped for both to ~0.5 Ω/Φ_n. It is interesting to notice that the change in resistivity of the 500-nm- and 1000-nm-thick samples are very similar, indicating no big impact of the thickness on the final device sensitivity. On the other hand, a dependence of the sensitivity on the geometry has been observed when comparing the two mentioned copper RDRs of PCB1, with respect to the other two copper RDRs on PCB2 (Cu-0.5u and Cu-1u of PCB2 in Fig. 6). The firsts are longer RDRs (more fingers, 51 instead of 31), but narrower (10 µm instead of 30 µm). This suggests that a greater sensitivity can be achieved by increasing the overall area of exposed metal (see different area layouts in Fig. 2(a) and (b), thus increasing the probability of a hit by an incoming particle.

B. Proton Irradiation at CERN-IRRAD

As mentioned in Section IV-D, this irradiation experiment started in June 2017 and since then, it has continuously being irradiated, cumulating about 5×10^{15}p/cm^2 every week, reaching 5.2×10^{16} p/cm^2 in September 2017.

Since the beam spot is about 10 mm in diameter, only the four RDRs located next to the connector are being irradiated, while the fifth RDR (on both PCBs is the chromium sample) is getting only the tails of the Gaussian distributed beam, thus negligible with respect to the total fluence collected by the other sensors. Not measuring the Cr samples allowed freeing channels for the readout of NTC temperature sensors [as shown in Fig. 3(b)]. In addition, one of the sensors (Al-0.5 of PCB1) experienced a failure after two months of irradiation at about 3.7×10^{16} p/cm^2. Therefore, only experimental data collected from the remaining seven sensors is discussed here. Fig. 7 shows this data expressed in change of resistance of the RDRs with increasing proton fluence. From the graph it is clear that first, thanks to the stable temperature (21 °C ±0.5 °C), in the IRRAD bunker (NTC curves in Fig. 7), no resistance variation can be attributed to temperature variations. Second, the impinging protons are inducing a noticeable damage successfully measurable in a variation of the resistance. Again the copper samples are the ones most affected by the protons, and in particular the 1-µm-thick copper RDR on PCB2 (Cu-1u) is showing the greater variation of almost 19% with respect to its starting resistance, while the aluminum samples stop at about 2.5%. Overall, in the range between 1×10^{16} and 5.2×10^{16} p/cm^2, the copper RDR of PCB2 have shown an initial sensitivity of ~2.1 Ω/Φ_preduced to ~0.68 Ω/Φ_p toward the end. The other copper RDRs have all about the same constant slope of ~1.2 Ω/Φ_p. The remaining aluminum RDRs stayed at 0% for almost half irradiation time, after which they started raising with a sensitivity of about ~0.1 Ω/Φ_p, where $\Phi_p = 10^{16}$ p/cm^2 for all the previously expressed sensitivities.

As also stated before for the neutron irradiation experiment, the thickness of the RDR does not affect greatly the dosimeter performance. On the other hand, the greater sensitivity could be attributed to the larger number of fingers (31 instead of 13),

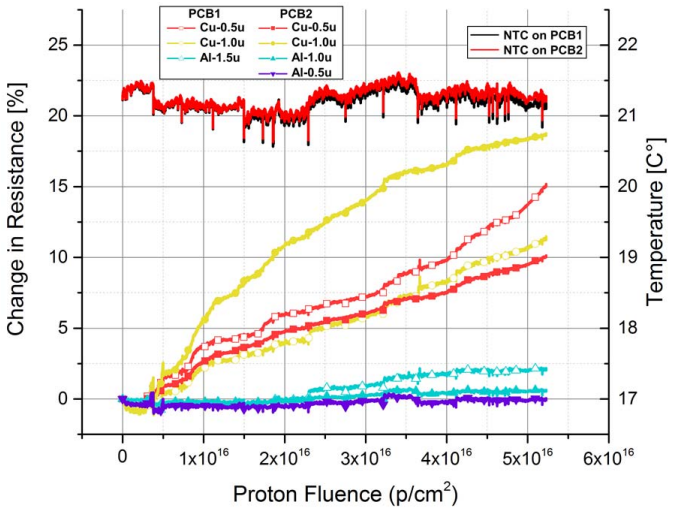

Fig. 7. Resistance variation from the initial value in percentage versus the integrated proton fluence over three months of irradiation (left y-axis). The noisy peaks observable at ~3.5×10^{16} p/cm^2, in the three PCB1 curves (pink, orange, and yellow) are results of the correction introduced to compensate the failures of the fourth sensor Al-0.5u of PCB1 (not plotted). On the right y-axis, the onboard temperature as measured by the two NTCs installed on each PCB.

but narrower (30 µm instead of 40 µm), once again suggesting that the top geometry, as well as the amount of exposed metal, are the key factors controlling the dosimeter sensitivity. Differently from the logarithmic dependence of the neutron irradiated RDRs, in this case all RDRs follow a nearly linear law, apart from the Cu-1u of PCB2, which seems to approach saturation.

VI. Discussion

The two irradiation tests were planned to cumulate as much displacement damage as possible. In the case of the neutron irradiation, thanks to the very high flux, the targeted FCC fluence has been reached and overtaken within five days. On the other hand, in the IRRAD Proton Facility, such high levels can be reached only after very long irradiation runs. While both irradiations qualify for testing material damage due to displacement, the very different particle types, energy spectra, and dose rates, do not allow for a straightforward comparison, and more irradiation data should be collected to find common scaling factors as it was done for silicon [32]. Furthermore, the very dissimilar irradiation conditions in terms of temperature, also introduce a fundamental point of divergence. In this context, the lack of temperature measurement on-board or of the irradiation channel during the neutron irradiation did not allow an appropriate data correction. Nevertheless, in the case of the copper samples, and in some extent also the aluminum RDRs, a clear constant increase is observable (in Figs. 5 and 7) thus meaning that the high irradiation temperature and the daily night stops did not always anneal completely the cumulated damage. Similarly in IRRAD, while no temperature problems have occurred, being kept stable (21 °C ± 0.5 °C), both copper (in much greater way) and aluminum, have shown a measurable increase in resistance with increasing fluence.

Considering the simulated DPA values shown in Table III, in the case of the proton irradiation, the values are very consistent with the measured data, since copper was correctly predicted to show about 5 times more DPA than for aluminum, and thus, the hypothesis that DPA is directly proportional to the increase of resistivity is verified.

On the other hand, the simulations performed for the DPA generated during neutron irradiation, seem to not correlate with the measurements. This discrepancy could be due to the strong temperature dependence of the resistivity variation in the measured data and this will be furthered investigated during a second neutron irradiation next year.

VII. Conclusion

An innovative dosimetry technology for very high fluence monitoring for the FCC at CERN has been discussed in this paper, describing its working principle based on radiation-induced permanent change in resistivity of metal thin film called RDRs).

A special rad-hard FCC-RADMON PCB has been designed for hosting several RDRs made of aluminum, chromium, and copper, of different sizes and with 1000- and 500-nm thicknesses, all entirely produced in cleanroom facilities.

Two irradiation tests have been performed: with neutrons, up to a total fluence of 1×10^{18} n/cm^2 at the MARK II TRIGA nuclear reactor of JSI in Ljubljana, and with 23-GeV protons, up to a total fluence of 5.2×10^{16} p/cm^2 at the IRRAD Proton Facility at CERN, Geneva.

The collected experimental data have shown a variation of resistivity with increasing particle fluence, confirming our concept of a dosimeter based on metal thin films. While no significant difference was found between the two chosen thin-film thicknesses, the variation in the sensitivity to displacement damage can be attributed to different geometries (number of fingers and their width). Even greater impact was observed for different materials: copper samples have shown the highest sensitivity for both irradiation tests, while aluminum and chromium samples exhibited a much weaker response.

Such material dependence has been confirmed by DPA simulations in the case of the proton irradiation, while for the neutron one, the excessive thermal annealing due to the >65 °C temperature reached in the reactor during irradiation, have potentially altered the net DPA, thus not matching the resistivity measurement.

A deeper understanding of the effects of very high particle fluence on thin metal films and in particular the physical mechanisms that lead to an increase of the resistivity will be the main focus of our future research.

As first, a larger amount of data will be available once the test in IRRAD will end in December 2017, cumulating a fluence of 1.2×10^{17} p/cm^2. In such way, we will have a wider view of the RDRs behavior over the whole FCC range. Second, another irradiation campaign will be performed in 2018 at the JSI TRIGA reactor, with FCC-RADMONs that have previously undergone a full electrical characterization in a climatic chamber, in order to extract the exact temperature coefficients of each device. This will allow fully understanding the effects of temperature on the metal structures, enabling to effectively disentangle the resistivity variation due to displacement from the one due to the temperature increase during irradiation.

In parallel, our research will focus on the basis of radiation damage on copper films, which have shown, in this paper, the best performance as dosimeters. This will be done by testing a wider range of samples, fabricated with different deposition techniques [physical vapor deposition, such as sputter and evaporator, and atomic layer deposition (ALD)], different etching procedures (wet etching, ion beam etching, and liftoff) and with different thicknesses (5 and 50 nm). In particular, in collaboration with the University of Helsinki, Helsinki, Finland, we are going to study the effects of nonionizing radiation on ALD copper films of few nanometres [33] extending the experimental work presented in this paper for thicker films of 1000 and 500 nm, down to films of 5 nm.

Acknowledgment

The authors would like to thank R. Froeschl from CERN-HSE/RP, Geneva, Switzerland, F. Cerutti from CERN-EN/STI, Geneva, and K. Ambrožič from JSI, Ljubljana, Slovenia, for the DPA simulations. They would also like to thank all the staff of the CMi cleanroom for their valuable support.

References

[1] A. Infantino, R. G. Alía, M. I. Besana, M. Brugger, and F. Cerutti, "Preliminary design of CERN Future Circular Collider tunnel: First evaluation of the radiation environment in critical areas for electronics," in *Proc. ICRS*, 2016, pp. 1–7, doi: http://doi.org/10.1051/epjconf/201715303004

[2] M. I. Besana, F. Cerutti, A. Ferrari, W. Riegler, and V. Vlachoudis, "Evaluation of the radiation field in the future circular collider detector," *Phys. Rev. Accel. Beams*, vol. 19, no. 11, p. 111004, 2016, doi: http://doi.org/10.1103/PhysRevAccelBeams.19.111004

[3] G. Apollinari, I. B. Alonso, O. Brüning, M. Lamont, and L. Rossi. (Dec. 2015). *High-Luminosity Large Hadron Collider (HL-LHC)*. [Online]. Available: http://cds.cern.ch/record/2116337

[4] B. Camanzi and A. G. Holmes-Siedle, "The race for new radiation monitors," *Nature Mater.*, vol. 7, no. 5, pp. 343–345, 2008, doi: http://doi.org/10.1038/nmat2159

[5] B. Gkotse, M. Glaser, P. Lima, E. Matli, M. Moll, and F. Ravotti, "A new high-intensity proton irradiation facility at the CERN PS east area," in *Proc. Sci.*, 2014, pp. 1–5. [Online]. Available: http://pos.sissa.it/213/354

[6] L. Snoj, G. Žerovnik, and A. Trkov, "Computational analysis of irradiation facilities at the JSI TRIGA reactor," *Appl. Radiat. Isotopes*, vol. 70, no. 3, pp. 483–488, Mar. 2012, doi: http://doi.org/10.1016/j.apradiso.2011.11.042

[7] F. Ravotti, M. Glaser, A. B. Rosenfeld, M. L. F. Lerch, A. G. Holmes-Siedle, and G. Sarrabayrouse, "Radiation monitoring in mixed environments at CERN: From the IRRAD6 facility to the LHC experiments," *IEEE Trans. Nucl. Sci.*, vol. 54, no. 4, pp. 1170–1177, Aug. 2007, http://doi.org/10.1109/TNS.2007.892677

[8] G. Spiezia *et al.*, "The LHC radiation monitoring system—RadMon," in *Proc. Sci.*, 2011, pp. 1–12. [Online]. Available: http://pos.sissa.it/archive/conferences/143/024/RD11_024.pdf

[9] F. Ravotti, M. Glaser, and M. Moll, "SENSOR CATALOGUE' data compilation of solid-state sensors for radiation monitoring," CERN, Geneva, Switzerland, Tech. Rep. CERN-TS-Note-2005-002, May 2005. [Online]. Available: http://cds.cern.ch/record/835408

[10] J. M. Swartz and M. O. Thurston, "Analysis of the effect of fast-neutron bombardment on the current-voltage characteristic of a conductivity-modulated *p-i-n* diode," *J. Appl. Phys.*, vol. 37, no. 2, pp. 745–755, 1966, doi: http://doi.org/10.1063/1.1708249

[11] M. M. Ramsay, "The effect of neutron irradiation on thin film resistors," *Thin Solid Films*, vol. 1, no. 6, pp. 405–416, May 1968, doi: http://doi.org/10.1016/0040-6090(68)90069-2

[12] J. Shewchun, W. R. Hardy, D. Kuenzig, and C. Tam, "Reactively sputtered tantalum thin film resistors Part 2. Low energy, low fluence proton radiation damage," *Thin Solid Films*, vol. 8, no. 2, pp. 101–115, Aug. 1971. [Online]. Available: https://doi.org/10.1016/0040-6090(71)90002-2

[13] K. Farrell and A. E. Richt, "Microstructure and tensile properties of heavily irradiated 1100-0 aluminum," in *Effects of Radiation on Structural Materials*, J. A. Sprague and D. Kramer, Eds. Philadelphia, PA, USA: ASTM, 1979, pp. 427–439. [Online]. Available: http://www.osti.gov/scitech/servlets/purl/6663374

[14] M. Kangilaski. (1967). *The Effects of Neutron Radiation on Structural Materials*. [Online]. Available: https://ntrs.nasa.gov/search.jsp?R=19680007407

[15] NASA. (Jun. 1970). *Nuclear and Space Radiation Effects on Materials, NASA Space Vehicle Design Criteria-(Structures)*. [Online]. Available: https://ntrs.nasa.gov/archive/nasa/casi.ntrs.nasa.gov/19710015558.pdf

[16] J. W. Martin, "The electrical resistivity of some lattice defects in FCC metals observed in radiation damage experiments," *J. Phys. F, Met. Phys.*, vol. 2, no. 5, pp. 842–853, 1972, doi: http://doi.org/10.1088/0305-4608/2/5/008

[17] S. J. Zinkle, "Electrical resistivity of small dislocation loops in irradiated copper," *J. Phys. F, Met. Phys.*, vol. 18, no. 3, pp. 377–391, 1988, doi: http://doi.org/10.1088/0305-4608/18/3/009

[18] M. Li, M. Eldrup, T. S. Byun, N. Hashimoto, L. L. Snead, and S. J. Zinkle, "Low temperature neutron irradiation effects on microstructure and tensile properties of molybdenum," *J. Nucl. Mater.*, vol. 376, no. 1, pp. 11–28, May 2008, doi: http://doi.org/10.1016/j.jnucmat.2007.12.001

[19] R. L. Chaplin and R. R. Coltman, Jr., "Defects and transmutations in reactor-irradiated copper," *J. Nucl. Mater.*, vols. 108–109, pp. 175–182, Jul./Aug. 1982, doi: http://doi.org/10.1016/0022-3115(82)90485-8

[20] R. B. Ross, *Metallic Materials Specification Handbook*, 4th ed. Boston, MA, USA: Springer, 1992. [Online]. Available: https://doi.org/10.1007/978-1-4615-3482-2

[21] F. Ravotti and R. Froeschl, private communication, Jan. 2017.

[22] J. F. Ziegler, M. D. Ziegler, and J. P. Biersack, "SRIM—The stopping and range of ions in matter (2010)," *Nucl. Instrum. Methods Phys. Res. Sec. B*, vol. 268, nos. 11–12, pp. 1818–1823, 2010. [Online]. Available: http://dtic.mil/dtic/tr/fulltext/u2/a515302.pdf

[23] A. Ferrari, P. R. Sala, A. Fasso, and J. Ranft, "FLUKA: A multi-particle transport code," CERN, Geneva, Switzerland, Tech. Rep. CERN-2005-10, 2005, [Online]. Available: http://cds.cern.ch/record/898301

[24] T. T. Böhlen *et al.*, "The FLUKA code: Developments and challenges for high energy and medical applications," *Nucl. Data Sheets*, vol. 120, pp. 211–214, Jun. 2014, doi: http://doi.org/10.1016/j.nds.2014.07.049

[25] A. Fasso, A. Ferrari, G. Smirnov, V. Vlachoudis, and F. Sommerer, "FLUKA realistic modeling of radiation induced damage," in *Proc. SNA + Monte Carlo*, Tokyo, Japan, 2010, p. 1630. [Online]. Available: http://inis.iaea.org/Search/search.aspx?orig_q=RN:43053566

[26] M. J. Norgett, M. T. Robinson, and I. M. Torrens, "A proposed method of calculating displacement dose rates," *Nucl. Eng. Design*, vol. 33, no. 1, pp. 50–54, Aug. 1975, doi: http://doi.org/10.1016/0029-5493(75)90035-7

[27] *CMI—Center of MicroNanoTechnology—EPFL*. Accessed: Dec. 23, 2017. [Online]. Available: https://cmi.epfl.ch/

[28] F. Ravotti *et al.*, "Conception of an integrated sensor for the radiation monitoring of the CMS experiment at the large hadron collider," *IEEE Trans. Nucl. Sci.*, vol. 51, no. 6, pp. 3642–3648, Dec. 2004, doi.org/10.1109/TNS.2004.839265.

[29] *Doosan Electronics, Halogen-Free Substrate Materials (DS-7402)*. Accessed: Dec. 23, 2017. [Online]. Available: http://www.doosanelectronics.com/en/halogen-free-substrate-materials/fr-4-ds-7402/

[30] G. Žerovnik *et al.*, "Validation of the neutron and gamma fields in the JSI TRIGA reactor using in-core fission and ionization chambers," *Appl. Radiat. Isotopes*, vol. 96, pp. 27–35, Feb. 2015, doi: http://doi.org/10.1016/j.apradiso.2014.10.026

[31] A. Curioni *et al.*, "Single- and multi-foils ^{27}Al(p,3pn)^{24}Na activation technique for monitoring the intensity of high-energy beams," *Nucl. Instrum. Methods Phys. Res. A, Accel. Spectrom. Detect. Assoc. Equip.*, vol. 858, pp. 101–105, Jun. 2017. [Online]. Available: http://linkinghub.elsevier.com/retrieve/pii/S0168900217304199

[32] G. Lindström, M. Moll, and E. Fretwurst, "Radiation hardness of silicon detectors—A challenge from high-energy physics," *Nucl. Instrum. Methods Phys. Res. A, Accel. Spectrom. Detect. Assoc. Equip.*, vol. 426, no. 1, pp. 1–15, Apr. 1999, doi: http://doi.org/10.1016/S0168-9002(98)01462-4

[33] K. Väyrynen *et al.*, "Low-temperature atomic layer deposition of low-resistivity copper thin films using Cu(dmap)$_2$ and tertiary butyl hydrazine," *Chem. Mater.*, vol. 29, no. 15, pp. 6502–6510, 2017, doi: http:doi.org/10.1021/acs.chemmater.7b02098

[34] K. Ambrožič, G. Žerovnik, and L. Snoj, "Computational analysis of the dose rates at JSI TRIGA reactor irradiation facilities," *Appl. Radiat. Isotopes*, vol. 130, pp. 140–152, Aug. 2017. [Online]. Available: https://doi.org/10.1016/j.apradiso.2017.09.022